IEEE Photonics Journal
An IEEE Photonics Society Publication

Open Access

Fractal Conical Lens Optical Tweezers

Volume 9, Number 1, February 2017

Zhirong Liu
Philip H. Jones

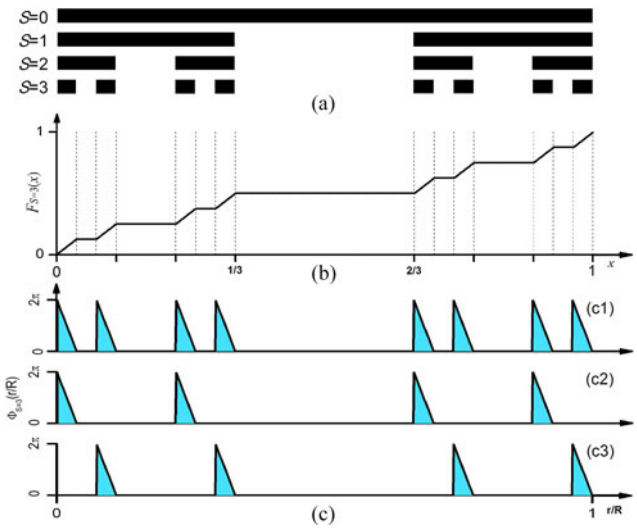

DOI: 10.1109/JPHOT.2016.2644966
1943-0655 © 2016 IEEE

IEEE photonics SOCIETY

IEEE

Fractal Conical Lens Optical Tweezers

Zhirong Liu[1,2] **and Philip H. Jones**[2]

[1]Department of Applied Physics, East China Jiaotong University, Nanchang 330013, China
[2]Department of Physics and Astronomy, University College London, London WC1E 6BT, U.K.

DOI:10.1109/JPHOT.2016.2644966

Manuscript received November 8, 2016; revised November 30, 2016; accepted December 16, 2016. Date of publication December 23, 2016; date of current version January 11, 2017. This work was supported in part by the National Natural Science Foundation of China under Grant 11547002, in part by the Jiangxi Provincial Natural Science Foundation of China under Grant 20161BAB201031, in part by the Scientific Project of Jiangxi Education Department of China under Grant GJJ150531, and in part by the China Scholarship Council under Grant 201508360027. Corresponding author: Z. Liu (e-mail: liuzhirong_2003@126.com).

Abstract: We propose a novel optical tweezers composed of an annular beam with alternate radially and azimuthally polarized rings modulated by a fractal conical lens (FCL) and demonstrate its optical forces on Rayleigh dielectric particles both analytically and numerically. Owing to the optical system's particular focusing properties, which could generate a dark-centered or peak-centered intensity distribution in the focal region when selecting an appropriate truncation parameter in front of the focusing lens, the proposed FCL optical tweezers could selectively trap and manipulate dielectric mesoscopic particles with low- or high-refractive indices by appropriately adjusting the radius of the pupil or the beam. Finally, the stability conditions for effective trapping and manipulation Rayleigh particles are analyzed.

Index Terms: Laser trapping, optical confinement and manipulation, propagation.

1. Introduction

Optical tweezers, which apply light's mechanical effect to trap and manipulate mesoscopic particles, nowadays have become a major area of cutting-edge science and application science since the seminal work by Ashkin in the 1970s [1]–[12]. It is known that photons carry momentum and energy. Through the exchange of momentum and energy between photons and the target particles, a laser beam can exert optical forces to the particles it encounters at near the intensity extreme points. A conventional optical tweezers setup is mainly constructed by highly focused fundamental Gaussian laser beams to attract high-refractive index particles (particles having a refractive index higher than that of the surrounding medium) into the focal region of the beam, and meanwhile, low-refractive index particles (particles having a refractive index lower than that of the surrounding medium) are expelled from the beam, in contrast. Recent studies have demonstrated that optical forces exerted on a particle depend crucially on the properties of the incident beam [6], [7], the particle itself [8], and the interaction between them (i.e. optical scattering). Therefore, to obtain the desired manipulation effect, one may increase the degree of control over the particles by controlling the key parameters of either the beam or the particle [8].

A fractal conical lens (FCL) is a newly proposed kind of fractal lens, in which the radial phase distribution is characterized by the Cantor function [13], [14]. Owing to its particular self-similarity

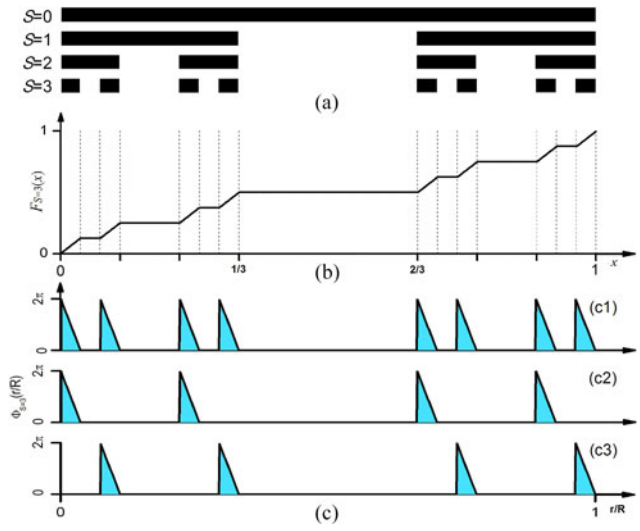

Fig. 1. (a) Generation of the triadic Cantor set, starting from the *initiator* $S = 0$ to $S = 3$. (b) Cantor function $F_S(x)$ for $S = 3$. (c) Phase of a triadic FCL for $\Phi_s = 2^{s+1}\pi F_s(\varsigma)$ with $S = 3$ and $\varsigma = r/R$. Phase of (c1) a triadic FCL. (c2) and (c3) Two *triadic-related* FCL divided from the triadic FCL.

properties under monochromatic illumination, research and applications of FCL focusing has attracted increasing interest in recent years [13]–[16]. In this paper we propose a novel optical tweezers, utilizing an annular beam with alternate radially and azimuthally polarized rings focused by a FCL. Due to the focusing optical field's special properties, which could generate a dark-centered or peak-centered intensity distribution in the focal region by selecting an appropriate truncation parameter β_0, defined as the ratio of the pupil radius R to the incident beam radius w_0 in front of the focusing lens, the proposed FCL optical tweezers can easily be tuned to selectively trap and manipulate dielectric micro-particles with low- or high-refractive indices by appropriately adjusting the radius of the pupil or the beam. Finally, the stability conditions for effective trapping and manipulation Rayleigh particles are analyzed.

2. Theory Model

As a newly proposed rotationally symmetric diffractive optical elements (DOE), the phase profile of a fractal conical lens (FCL) is generated from a Cantor set (CS) of a given stage S. As an example, Fig. 1(a) illustrates the construction of a regular triadic CS. The first step in the FCL construction procedure, consists in defining a straight-line segment of unit length called the *initiator* (stage $S = 0$). Next, at stage $S = 1$, the *generator* of the set is constructed by dividing the segment into three equal parts of length 1/3 and removing the central one. Following this procedure at the subsequent stages $S = 2, 3, \ldots$ is easy to see that, in general, at stage S, there are 2^S segments of length 3^{-S} with 2^S-1 disjoint gaps located at the intervals $[p_{s,l}, q_{s,l}]$, with $l = 1, \ldots, 2^S - 1$. For instance, for $S = 3$, the triadic CS presents seven gaps at [1/27, 2/27], [3/27, 6/27], [7/27, 8/27], [9/27, 18/27], [19/27, 20/27], [21/27, 24/27], and [25/27, 26/27]. For clarity, the three first stages CS are shown in Fig. 1(a) and (b) (a similar procedure could be followed for CS other than triadic).

Based on the fractal structure, the Cantor function $F_S(x)$ can be defined in the domain [0, 1] as [13], [14]

$$F_S(x) = \begin{cases} \dfrac{l}{2^S} & \text{if } p_{S,l} \le x \le q_{S,l} \\ \dfrac{1}{2^S}\dfrac{x - q_{S,l}}{p_{S,l+1} - q_{S,l}} + \dfrac{l}{2^S} & \text{if } q_{S,l} \le x \le p_{S,l+1} \end{cases} \tag{1}$$

with $l = 1, \ldots, 2S-1$, and $F_S(0) = 0$, $F_S(1) = 1$. For example, for $S = 3$ [see Fig. 1(a)], on the intervals, the constant values of $F_3(x)$ are 1/8, 2/8, 3/8, 4/8, 5/8, 6/8, and 7/8, respectively. In between these intervals the continuous function increases linearly as plotted in Fig. 1(b).

From the definition of Cantor function $F_S(x)$, one obtains that FCL is a rotationally symmetric pupil with phase profile following the Cantor function at a given stage S. At the gap intervals $[p_{sl}, q_{sl}]$ the phase shift is $-l2\pi$ with $l = 1, \ldots, 2^S - 1$. Then, the phase profile of a FCL of order S is given by

$$q(\varsigma) = q_{\mathrm{FCL}}(\varsigma, S) = \exp\left[-\mathrm{i}2^{S+1}\pi F_S(\varsigma)\right] \tag{2}$$

where

$$\varsigma = r/R \tag{3}$$

is the radial variable r normalized by the pupil radius R. Then, the surface-relief profile of the FCL can be expressed from the relation [16]

$$h_{\mathrm{FCL}}(r) = \mathrm{mod}_{2\pi}\left[-2^{s+1}\pi F_S\left(\frac{r}{R}\right)\right]\frac{\lambda}{2\pi(n-1)} \tag{4}$$

where $\mathrm{mod}_{2\pi}[\varphi(r)]$ denotes the phase function $\varphi(r)$ modulo 2π, n represents the refractive index of the optical material used for constructing the lens, and λ is the wavelength of the light.

Fig. 1(c1) depicts the profile of a triadic FCL generated by (4) in the case $S = 3$. It is obvious that there exist eight phase peaks in the domain [0, 1] along the radial direction. Fig. 1(c2) and (c3) show the profiles of two sets of *triadic-related* FCL, which are divided from the above triadic FCL and will be, respectively, used to modulate the radially polarized and the azimuthally polarized components of the incident beam in the following analysis. Obviously, phase distribution of Fig. 1(c1) is the sum of the alternate phase distributions of Fig. 1(c2) and (c3).

When illuminated by an incident light beam, the transmittance of a FCL can be expressed as

$$T(\theta) = \exp\left[-\mathrm{i}2^{S+1}\pi F_S\left(\frac{\sin\theta}{\sin\alpha}\right)\right] \tag{5}$$

where $\alpha = \sin^{-1}(NA/n_1)$ represents the maximum convergence angle determined by NA and n_1; here, NA is the objective lens' numerical aperture, and n_1 is the refractive index in image space.

According to the vectorial Debye theory, when the alternate radially- and azimuthally-polarized beams modulated by a FCL is focused by a high NA objective, the radial, longitudinal and azimuthal components of the electric field in the focal region, respectively, have the form [18], [19]

$$E_r(\rho, z) = A\int_0^{\alpha}\cos^{1/2}\theta\sin(2\theta)l_0(\theta)T_1(\theta)J_1(k\rho\sin\theta)e^{\mathrm{i}kz\cos\theta}d\theta \tag{6a}$$

$$E_z(\rho, z) = 2iA\int_0^{\alpha}\cos^{1/2}\theta\sin^2\theta l_0(\theta)T_1(\theta)J_0(k\rho\sin\theta)e^{\mathrm{i}kz\cos\theta}d\theta \tag{6b}$$

$$E_\phi(\rho, z) = 2A\int_0^{\alpha}\cos^{1/2}\theta\sin(\theta)l_0(\theta)T_2(\theta)J_1(k\rho\sin\theta)e^{\mathrm{i}kz\cos\theta}d\theta \tag{6c}$$

where $A = \pi f\sqrt{n_1}/\lambda$ denotes a constant with f, n_1 and λ being the optical focal length, refractive index of the medium, and optical length in vacuum, respectively. $l_0(\theta)$ represents the amplitude of the field in the pupil of the lens assumed to be a function of θ only. $k = 2\pi n_1/\lambda$ denotes the wave number in image space, J_0 and J_1 represent Bessel functions of the first kind of orders 0 and 1, respectively. In addition, $T_1(\theta)$ and $T_2(\theta)$ denote transmittance of two sets of *triadic-related* FCL shown in Fig. 1(c2) and (c3), which are divided from a triadic FCL and used to modulate the radially and azimuthally polarized components of the incident beam, respectively.

In the following analysis, it is supposed that the radially and azimuthally polarized components of the incident beam have a Laguerre Gaussian profile [20]

$$l_0(\theta) = E_0\beta_0\frac{\sin\theta}{\sin\alpha}\exp\left[-\left(\beta_0\frac{\sin\theta}{\sin\alpha}\right)^2\right]L_p^1\left[2\left(\beta_0\frac{\sin\theta}{\sin\alpha}\right)^2\right] \tag{7}$$

where

$$E_0 = \sqrt{4\beta_0^2 P_0/[(p+1)\pi w_0^2]} \tag{8}$$

is a constant related to the incident beam power P_0, and L_p^1 represents the generalized Laguerre polynomial with p+1 rings. $w_0 = f\sin\alpha$ is the beam width, and β_0 is a truncation parameter, which denotes the ratio of the pupil radius R to the incident beam radius w_0 in front of the focusing lens. Note that β_0 should be greater than 1 because some intensity distribution of the incident optical beam would be blocked by the pupil if $\beta_0 < 1$.

Thus, the total intensity distribution of light beams in the focal region can be expressed as

$$I(\rho, z) = \left|E_r(\rho, z)\right|^2 + \left|E_z(\rho, z)\right|^2 + \left|E_\phi(\rho, z)\right|^2. \tag{9}$$

In terms of (5)–(9), evolution of the optical intensity distribution of highly focused alternate radially and azimuthally polarized beams modulated by a FCL can be examined.

In this work, a Rayleigh dielectric sphere is considered as the target particle in the following analysis of radiation forces. Under this condition, the micro-sized dielectric sphere can be regarded as a simple induced dipole, and two types of radiation forces are identified in the highly focused optical field: scattering force $\vec{F}_{scat}$ and gradient force $\vec{F}_{grad}$ [2]. The gradient force arises from the inhomogeneous electromagnetic field distribution [18] and is responsible for pulling the target particles towards the optical equilibrium point. The scattering force is due to the net momentum transfer between the photons and the particles, and tends to push the particles out of the equilibrium point and even destabilize the optical trap. Then the scattering force is expressed as [22]

$$\vec{F}_{scat}(r, z) = \hat{z}\frac{n_1}{c}C_{scat}\langle S\rangle_z \tag{10}$$

where $\hat{z}$ denotes the unit vector along with beam propagation, and $c = 1/\sqrt{\varepsilon_0\mu_0}$ represents the speed of the light in vacuum, with ε_0 and μ_0 being the dielectric constant and the magnetic permeability in the vacuum, respectively. $\langle S\rangle_z = \mathrm{Re}\{(\vec{E}\times\vec{H}^*)_z\}/2 = \mathrm{Re}\{E_r H_\phi^*\}/2$ denotes the time averaged axial component of the Poynting vector, C_{scat} represents the cross section of radiation pressure for the interaction between light beam and micro-sized sphere. Within the Rayleigh approximation, the coefficient C_{scat} is defined by [23]

$$C_{scat} = \frac{8}{3}\pi(ka)^4 a^2\left(\frac{m^2-1}{m^2+2}\right)^2 \tag{11}$$

where $m = n_2/n_1$ denotes the relative refractive index, and n_2 and a is the refractive index and radius of the particle, respectively. The gradient forces along the transverse (radial) and axial (longitudinal) directions are, respectively, given by [24]

$$\vec{F}_{gradr}(r, z) = \frac{2\pi n_1 a^3}{c}\left(\frac{m^2-1}{m^2+2}\right)\frac{\partial}{\partial r}I(r, z) \tag{12}$$

$$\vec{F}_{gradz}(r, z) = \frac{2\pi n_1 a^3}{c}\left(\frac{m^2-1}{m^2+2}\right)\frac{\partial}{\partial z}I(r, z). \tag{13}$$

Equations (5)–(13) provide a general description of the focusing properties and radiation forces exerting on a Rayleigh particle by highly focused alternate radially and azimuthally polarized beams modulated by a FCL. Without loss of generality, in the following simulations the parameters are selected as: $\lambda = 632.8$ nm, $a = 30$ nm, $f = 1$ mm, $w_0 = 1$ mm, $n_1 = 1.33$, $NA = 1$, $p = 1$, and the laser beam power P_0 is assumed to be 1W.

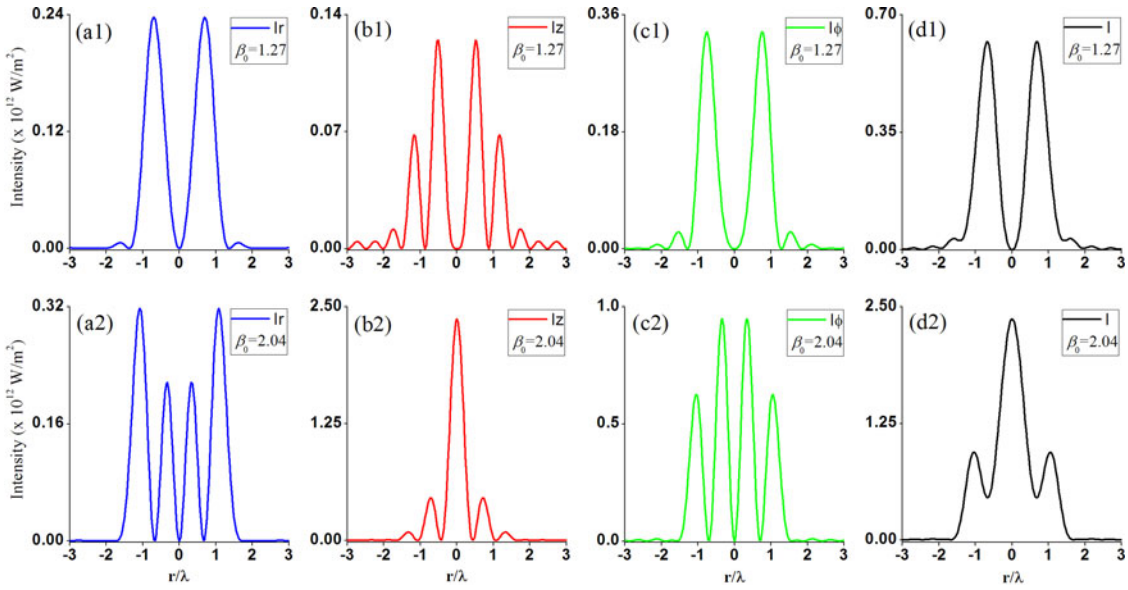

Fig. 2. Intensity profiles of (a1) and (a2) radial component, (b1) and (b2) longitudinal component, (c1) and (c2) azimuthal component, and (d1) and (d2) the total intensity distribution in the focal plane ($z = 0$) for $\beta_0 = 1.27$ (upper row) and $\beta_0 = 2.04$ (lower row). The total beam power in each transverse plane is normalized to $P_0 = 1$ W.

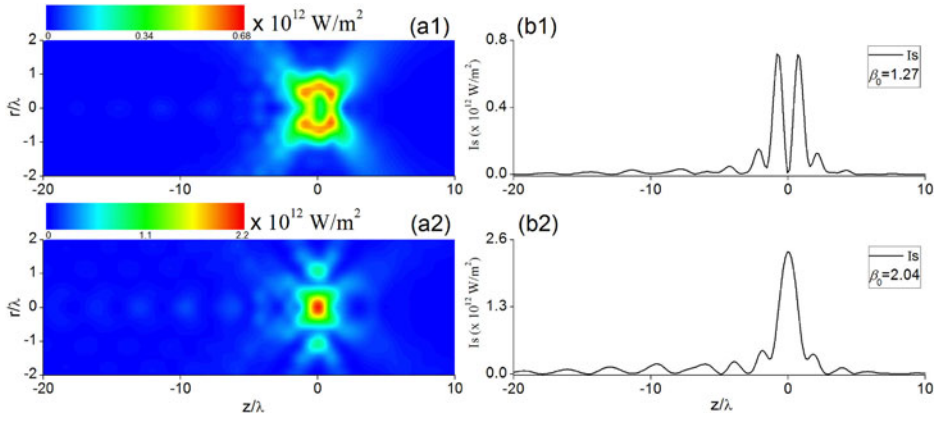

Fig. 3. Total intensity distributions I(ρ, z) (2-D in the left column and 1-D in the right column) in the longitudinal plane for $\beta_0 = 1.27$ (upper row) and $\beta_0 = 2.04$ (lower row). The beam power in each transverse plane is normalized to $P_0 = 1$ W.

3. Numerical Simulations and Analysis

3.1 Focusing Properties

Fig. 2 shows the intensity profiles of each component in the focal plane ($z = 0$) for values of the truncation parameter $\beta_0 = 1.27$ (upper row) and $\beta_0 = 2.04$ (lower row), respectively. It is clear that both the radial components (see Fig. 2(a1) and (a2)) and the azimuthal components (see Fig. 2(c1) and (c2)) on the beam axis (r = 0) are null for both values of β_0. For $\beta_0 = 1.27$, however, the longitudinal component (see Fig. 2(b1)) has a null distribution on the axis and the total intensity (see Fig. 2(d1)) forms a dark-centered distribution, which is the so-called "optical cage"; for $\beta_0 = 2.04$, the longitudinal component (see Fig. 2(b2)) presents a maximum value on the axis and the total intensity (see Fig. 2(d2)) generates a rather different peak-centered distribution.

Fig. 3 illustrates the evolution of the total intensity distributions $I(\rho, z)$ (2-D in the left column and 1-D in the right column) in the longitudinal plane for $\beta_0 = 1.27$ (upper row) and $\beta_0 = 2.04$ (lower

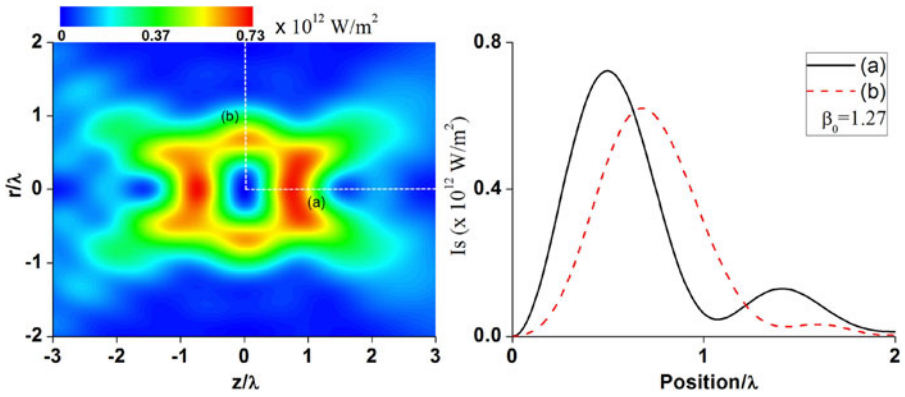

Fig. 4. Intensity distribution for $\beta_0 = 1.27$ through the focus with intensity profiles along (a) the axial direction and (b) the radial direction. Each intensity profile is normalized to the incident beam power $P_0 = 1$ W.

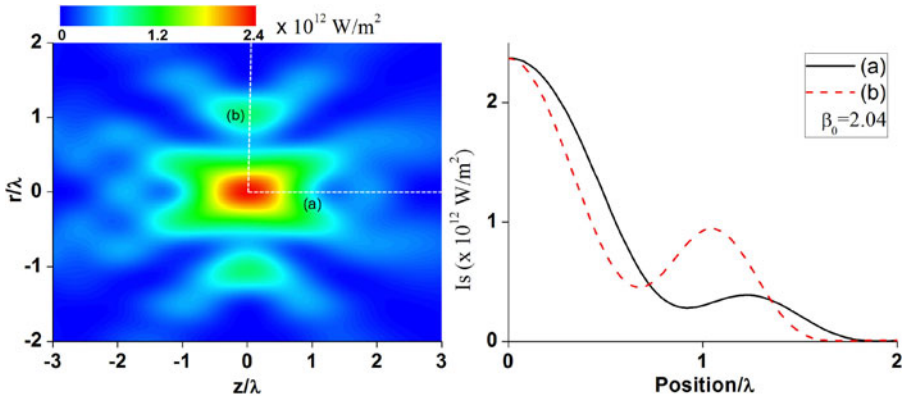

Fig. 5. Intensity distribution for $\beta_0 = 2.04$ through the focus with intensity profiles along (a) the axial direction and (b) the radial direction. Each intensity profile is normalized to the incident beam power $P_0 = 1$ W.

row), respectively. As one can find from Fig. 3, besides the above-mentioned different intensity distributions in the focal plane ($z = 0$), evolution of the total intensity $I(\rho, z)$ share the common self-similarity diffractive properties for both values of $\beta_0 = 1.27$ and 2.04, which are characteristic of the FCL.

In order to clearly demonstrate the optical field configuration in the focal region, Figs. 4 and 5 depict the intensity distributions for $\beta_0 = 1.27$ and $\beta_0 = 2.04$, respectively. It is clearly seen that, for $\beta_0 = 1.27$, a three-dimensional dark spot (i.e. optical cage) emerges in the focal region, which can be testified by the insets Fig. 4(a) and (b); while for $\beta_0 = 2.04$, it is a three-dimensional bright spot in the focal region, which can be testified by Fig. 5(a) and (b).

Fig. 6(a) and (b) exhibit the intensity profiles in the focal plane ($z = 0$) for $\beta_0 = 1.27$ and $\beta_0 = 2.04$, respectively. The total beam power in each transverse plane is normalized to the incident beam power $P_0 = 1$ W. It is obvious from Fig. 6 that longitudinal components (dotted curves) vary drastically with different β_0. As a result, truncation parameter β_0 takes a key role in determining the construction of the total intensity distribution. It indicates that one may tailor the optical system's focusing properties by selecting an appropriate truncation parameter, which is of great usefulness in optical confinement and manipulation.

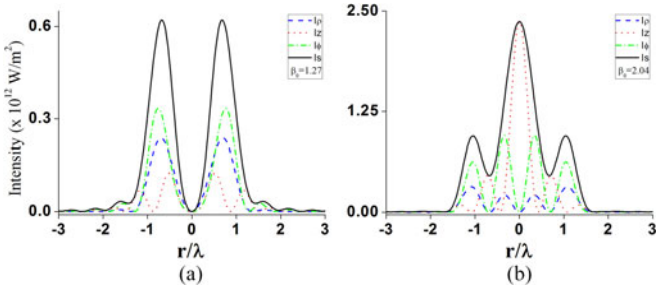

Fig. 6. Intensity profiles in the focal plane (z = 0) for (a) $\beta_0 = 1.27$ and (b) $\beta_0 = 2.04$. The radial component (dashed curve), longitudinal component (dotted curve), azimuthal component (dotted-dashed curve), and the total intensity (solid curve) are depicted in each figure. The total beam power in each transverse plane is normalized to the incident beam power $P_0 = 1$ W.

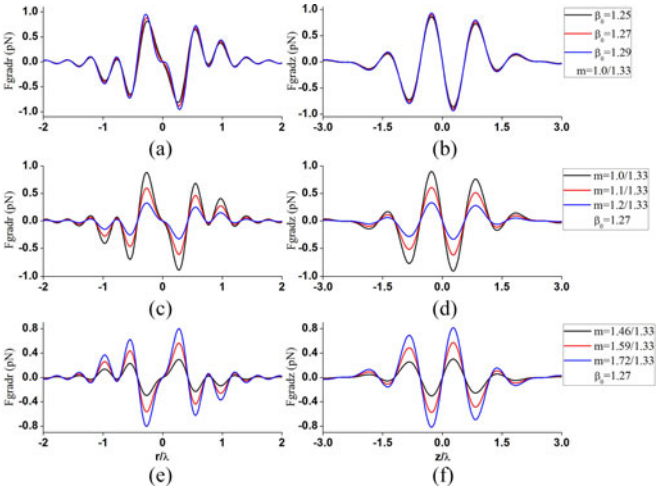

Fig. 7. Transverse gradient force $\vec{F}gradr$ (a), (c), (e) and the axial gradient force $\vec{F}gradz$ (b), (d), (f) acting on a Rayleigh particle with low-relative refractive index (m<1) or high-relative refractive index (m>1) generated by FCL optical tweezers.

3.2 Fractal Conical Lens Optical Tweezers' Optical Forces on Rayleigh Particles

According to the above analysis, one obtains that when $\beta_0 = 1.27$, the intensity distribution produces an optical cage in the focal region; thus, in this case, the FCL tweezers might trap and manipulate low-refractive index (m<1) Rayleigh particles at the focus and, simultaneously, high-refractive index (m>1) Rayleigh particles nearby the focus. In this section, we demonstrate FCL optical tweezers' optical forces on Rayleigh particles with high- and low-refractive indices. Fig. 7(a), (c), and (e) show FCL optical tweezers' transverse gradient force $\vec{F}gradr$, and Fig. 7(b), (d), and (f) longitudinal gradient force $\vec{F}gradz$, respectively, in dark-centered intensity distribution case. From Fig. 7(a)–(d), one finds that there exists one stable equilibrium point at the focal point for particles with low-refractive index (m<1), moreover, the optical forces become larger when decreasing the relative-refractive index m. Similarly, seen from Fig. 7(e) and (f), for high-refractive (m>1) particles, two stable equilibrium points are just located at the position of the two intensity sharp peaks, and the optical forces become larger when increasing the relative-refractive index m.

Fig. 8(a) and (c) illustrate FCL optical tweezers' transverse gradient force $\vec{F}gradr$, and Fig. 8(b) and (d) longitudinal gradient force $\vec{F}gradz$, respectively, in peak-centered intensity distribution case. It can been seen from Fig. 8 that there is one stable equilibrium point at the focal point for particles

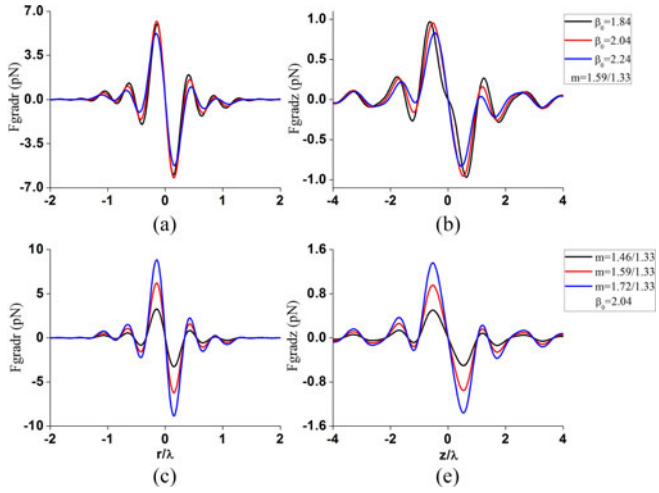

Fig. 8. Radial gradient forces $\vec{F}gradr$ (a), (c) and the axial gradient force $\vec{F}gradz$ (b), (d) acting on a Rayleigh particle with both high-relative (upper row) and low-relative (lower row) refractive index generated by FCL optical tweezers.

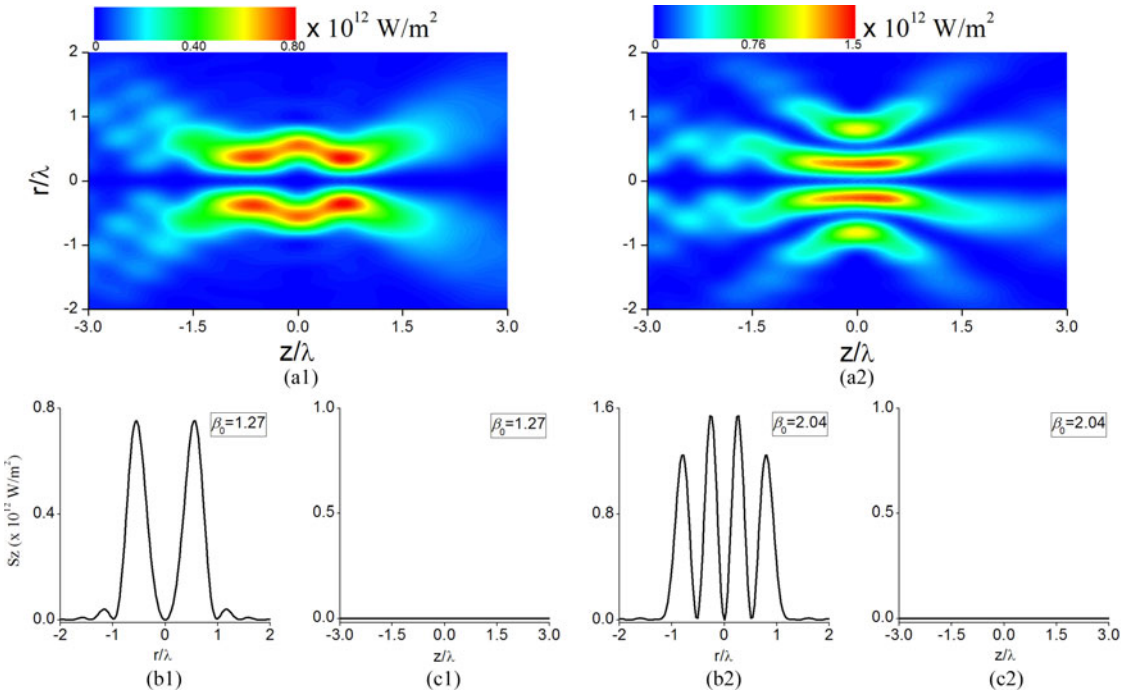

Fig. 9. Calculated axial component of time averaged Poynting vector $<S>_z$ for $\beta_0 = 1.27$ (left column) and $\beta_0 = 2.04$ (right column), and $< S >_z$ profiles (b1), (b2) along the radial direction, and (c1), (c2) along the axial direction through the focus.

with high-refractive index (m>1), and additionally, one can find from Fig. 8(c) and (d) that the optical forces become larger when increasing the relative-refractive index m.

Besides gradient forces $\vec{F}grad$, scattering force $\vec{F}scat$ is another kind of optical force existing in common optical tweezers. Based on (10), $\vec{F}scat$ is closely related to the axial component of optical field Poynting vector $< S >_z$. Fig. 9 exhibits the calculated $< S >_z$ for $\beta_0 = 1.27$ (left column) and $\beta_0 = 2.04$ (right column), respectively. Compared Figs. 4 and 5 with Fig. 9, one can find interesting

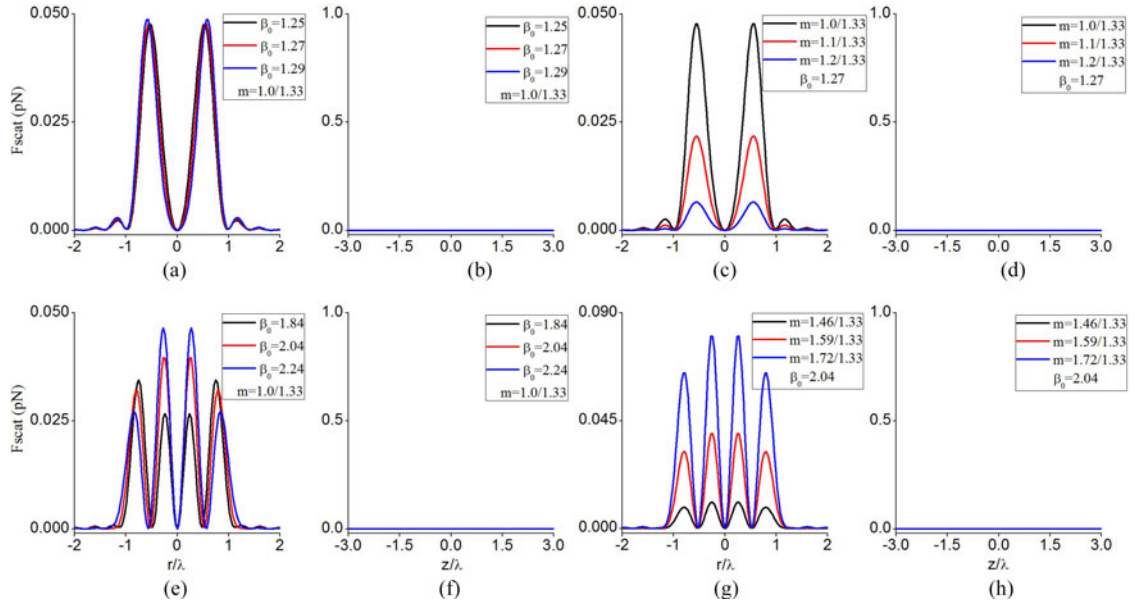

Fig. 10. Scattering force $\vec{F}scat$ acting on a Rayleigh particle with low- or high-relative refractive index generated by FCL optical tweezers.

features that although the parameters are the same, distributions of I_s and $<S>_z$ are rather different because the total intensity distribution I_s includes the axial field component I_z (see (9)), while I_z does not contribute to the Poynting vector $< S >_z$ along the optical axis [25].

Fig. 10 presents the FCL optical tweezers' scattering force $\vec{F}scat$ acting on a Rayleigh particle with both low- and high-relative refractive indices. Compared Fig. 10 with Fig. 9, it is easy to find that distribution of $\vec{F}scat$ is similar to that of $< S >_z$. Here, it is also worthy to point that the FCL optical tweezers' scattering force $\vec{F}scat$ drastically decrease because the strong axial field component I_z does not contribute to the scattering force $\vec{F}scat$, which is of great usefulness to stable confinement and manipulation.

4. Trapping Stability Analysis

From the above analysis, one may have the idea that the FCL optical tweezers may be utilized to selectively trap and manipulate dielectric Rayleigh particles with low- or high-refractive indices by selecting a proper truncation parameter β_0, which can be actualized by simply adjusting the radius R of a circular pupil inserted in front of the focusing lens. In order to stably trap particles under Rayleigh approximation, two necessary factors are required to fulfill: 1) The backward gradient force (i.e. axial gradient force) must be greater than the forward scattering force in the point of maximum axial gradient, i.e., $M = |\vec{F}gradz|/|\vec{F}scat| \geq 1$ [2], where the ratio M is called the stability criterion. Compare Fig. 8 and Fig. 10 one can easily find that at the same condition, magnitude of the axial gradient force is much greater than that of the scattering force (about 20 to 30 times greater). Therefore, the first stability criterion is well fulfilled. 2) Since the micro-particles are immersed in a liquid medium (for example water), its motion could strongly be influenced by Brownian motion. For this reason, to stably capture the micro-particles, a potential well induced by the optical gradient force must be deep enough to overcome the particles' kinetic energy due to thermal fluctuation, and this condition can be expressed by the Boltzmann factor [2]

$$R_{\text{thermal}} = \exp(-U_{\max}/k_B T) \ll 1 \tag{14}$$

where $U_{max} = \pi\varepsilon_0 n_1^2 a^3 |(m^2-1)/(m^2+2)| \cdot |\vec{E}_{max}|^2$ denotes the maximum depth of the potential well, k_B denotes Boltzmann constant, and T is the absolute temperature of the ambient. In the above numerical examples, at a room temperature $T = 300K$, for the low- and high-refractive index particles ($n_2 = 1.0$ and 1.59, respectively), the value of $R_{thermal}$ at the maximum intensity for $\beta_0 = 1.27$, and 2.04 is about $R_{thermal} \approx 1.5 \times 10^{-10}$, and 2.0×10^{-24}, respectively. Obviously, in both cases, the Boltzmann factors near the focal point are extremely small. Therefore, in our case the Brownian motion can be overcome and the particles can be stably captured. In all, in our case both low- and high-refractive index particles with radius $a \leq 30$nm can be stably trapped and manipulated by the FCL optical tweezers.

5. Conclusion

In conclusion, we have proposed a novel fractal conical lens (FCL) optical tweezers, which are composed of an annular beam with alternate radially and azimuthally polarized rings modulated by a fractal conical lens, and have demonstrated its optical forces on a Rayleigh particle both analytically and numerically. Results show that fractal conical lens optical tweezers can selectively trap and manipulate dielectric Rayleigh particles with low- or high-refractive indices by appropriately adjusting the radius of the pupil or the beam, which is convenient to operate in experiment. Finally, the stability conditions for effective trapping and manipulation Rayleigh particles are analyzed. The results obtained here are interesting and of usefulness in possible applications in optical confinement and manipulation, sorting micro-particles, and making use of a fractal conical lens.

Acknowledgment

The authors would like to thank the Editors/Reviewers for their constructive and helpful comments and suggestions for the paper.

References

[1] A. Ashkin, "Acceleration and trapping of particles by radiation pressure," *Phys. Rev. Lett.* vol. 24, no. 4, pp. 156–159, 1970.
[2] A. Ashkin, J. M. Dziedzic, J. E. Bjorkholm, and S. Chu, "Observation of a single-beam gradient force optical trap for dielectric particles," *Opt. Lett.* vol. 11, no. 5, pp. 288–290, May 1986.
[3] A. Ashkin, "Optical trapping and manipulation of neutral particles using lasers," *Proc. Nal. Acad. Sci. USA*, vol. 94, no. 10, pp. 4853–4860, May 1997.
[4] A. Ashkin, *Optical Trapping and Manipulation of Neutral Particles Using Lasers*. Hackensack, NJ, USA: World Scientific, 2006.
[5] A. N. Grigorenko, N. W. Roberts, M. R. Dickinson, and Y. Zhang, "Nanometric optical tweezers based on nanostructured substrates," *Nature Photon.*, vol. 2, no. 6, pp. 365–370, Jun. 2008.
[6] M. Padgett and R. Bowman, "Tweezers with a twist," *Nature Photon.*, vol. 5, no. 6, pp. 343–348, Jun. 2011.
[7] P. H. Jones, O. M. Maragò, and G. Volpe, *Optical Tweezers: Principles and Applications*. Cambridge, U.K.: Cambridge Univ. Press, 2015.
[8] S. E. S. Spesyvtseva and K. Dholakia, "Trapping in a material world," *ACS Photon.*, vol. 3, no. 5, pp. 719–736, May 2016.
[9] F. Merola *et al.*, "Simultaneous optical manipulation, 3-D tracking, and Imaging of micro-objects by digital holography in microfluidics," *IEEE Photon. J.* vol. 4, no. 2, pp. 451–454, Apr. 2012.
[10] T. Cao, L. Zhang, and M. J. Cryan, "Optical forces in metal/dielectric/metal fishnet metamaterials in the visible wavelength regime," *IEEE Photon. J.*, vol. 4, no. 5, pp. 1861–1869, Oct. 2012.
[11] G. Xiao, K. Yang, H. Luo, X. Chen, and W. Xiong, "Orbital rotation of trapped particle in a transversely misaligned dual-fiber optical trap," *IEEE Photon. J.* vol. 8, no. 1, Feb. 2016, Art. no. 6100108.
[12] S. Cheng, X. Zhang, W. Ma, and S. Tao, "Fractal zone plate beam based optical tweezers," *Sci. Rep.*, vol. 6, Sep. 2016, Art. no. 34492.
[13] D. R. Chalice, "A characterization of the cantor function," *Amer. Math. Monthly*, vol. 98, no. 3, pp. 255–258, Mar. 1991.
[14] J. A. Monsoriu, W. D. Furlan, P. Andrés, and J. Lancis, "Fractal conical lenses," *Opt. Exp.*, vol. 14, no. 20, pp. 9077–9082, Oct. 2006.
[15] J. A. Monsoriu, C. J. Zapata-Rodrguez, and W. D. Furlan, "Fractal axicons," *Opt. Commun.* vol. 263, no. 1, pp. 1–5, Jul. 2006.
[16] Y. Z. Yu and W. B. Dou, "Properties of approximate Bessel beams at millimeter wavelengths generated by fractal conical lens," *Prog. Electromagn. Res.*, vol. 87, pp. 105–115, 2008.

[17] Y. Han, L. N. Hazra, and C. A. Delisle, "Exact surface-relief profile of a kinoform lens from its phase function," *J. Opt. Soc. Amer. A*, vol. 12, no. 3, pp. 524–529, Mar. 1995.
[18] B. Richards and E. Wolf, "Electromagnetic diffraction in optical systems. 2. structure of the image field in an aplanatic system," *Proc. Roy. Soc. Lond. A*, vol. 253, no. 1274, pp. 358–379, 1959.
[19] K. S. Youngworth and T. G. Brown, "Focusing of high numerical aperture cylindrical-vector beams," *Opt. Exp.*, vol. 7, no. 2, pp. 77–87, Jul. 2000.
[20] S. Quabis, R. Dorn, M. Eberler, O. Glöckl, and G. Leuchs, "The focus of light-theoretical calculation and experimental tomographic reconstruction," *Appl. Phys. B, Lasers Opt.*, vol. 72, no. 1, pp. 109–113, Jan. 2001.
[21] Y. Harada and T. Asakura, "Radiation forces on a dielectric sphere in the Rayleigh scattering regime," *Opt. Commun.* vol. 124, no. 5–6, pp. 529–541, Mar. 1996.
[22] K. Visscher and G. J. Brakenhoff, "A theoretical study of optically induced forces on spherical particles in a single beam trap. 1. Rayleigh scatterers," *Optik*, vol. 89, no. 4, pp. 174–180, Feb. 1992.
[23] M. Kerker, *The Scattering of Light and Other Electromagnetic Radiation*. New York, NY, USA: Academic, 1969.
[24] J. A. Stratton, *Electromagnetic Theory*. New York, NY, USA: McGraw-Hill, 1941.
[25] Q. Zhan, "Trapping metallic Rayleigh particles with radial polarization," *Opt. Exp.*, vol. 12, no. 15, pp. 3377–3382, Jul. 2004.